Nanoscale

PAPER

View Article Online
View Journal | View Issue

Cite this: *Nanoscale*, 2023, **15**, 3188

Renal-clearable porous hollow copper iron oxide nanoparticles for trimodal chemodynamic-photothermal-chemo anti-tumor therapy†

Kai Feng,‡[a] Zhengtao Xu,‡[b] Yuhan Wang,[c] Xiyao Wu,[a] Fucheng Xiong,[b] Yiling Ruan,[a] Xiaojing Wu,[a] Linqian Ye,[a] Dong Su,[c] Jing Yu *[b] and Xiaolian Sun *[a]

Multifunctional nanoplatforms with the synergistic effects of multiple therapeutic modalities have become a research focus due to their superior anti-tumor properties over single therapeutic modalities. Herein, we developed around 14 nm porous hollow copper iron oxide nanoparticles (PHCuFeNPs) with pore sizes of around 2–3 nm as a cisplatin carrier and photothermal therapeutic agent. The PHCuFeNPs were synthesized *via* a galvanic reaction between Cu_2S nanoparticles and iron pentacarbonyl ($Fe(CO)_5$) followed by etching in the organic phase to make the pores. They were stable under normal physiological conditions, but the pores were etched in a weak acidic tumor microenvironment, resulting in the controlled release of Cu and Fe ions for enhanced chemodynamic therapy and accelerated cisplatin release for chemotherapy. Under 980 nm laser irradiation, the PHCuFeNPs could effectively heat up to further promote the release process for synergistic therapy. Besides, they were proved to mediate immunogenic cell death to activate the immune system for potential immunotherapy. Together with their ability to degrade into fragments for fast renal metabolism, we believe that these PHCuFeNPs could provide a biocompatible and efficient multi-antitumor therapeutic approach.

Received 7th November 2022,
Accepted 1st January 2023

DOI: 10.1039/d2nr06224k

rsc.li/nanoscale

[a]*State Key Laboratory of Natural Medicines, Key Laboratory of Drug Quality Control and Pharmacovigilance, Department of Pharmaceutics, China Pharmaceutical University, Nanjing 210009, China. E-mail: xiaolian_sun@cpu.edu.cn*
[b]*College of Materials Science and Engineering, Zhejiang University of Technology, Hangzhou 310014, China*
[c]*Beijing National Laboratory for Condensed Matter Physics, Institute of Physics, Chinese Academy of Sciences, 100190 Beijing, China*

†Electronic supplementary information (ESI) available. See DOI: https://doi.org/10.1039/d2nr06224k

‡These two authors contributed equally to this research.

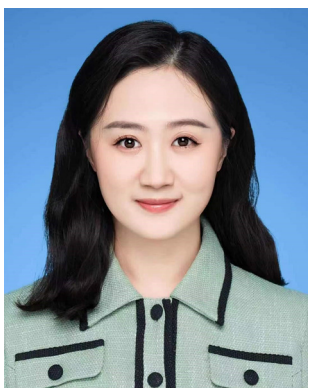

Xiaolian Sun

Professor Xiaolian Sun obtained her B.S. degree in chemistry from Nanjing University and PhD from Brown University, followed by postdoc training in the National Institutes of Health. Currently, she is a full professor at China Pharmaceutical University. Her research interests are focused on the biomedical application of nanomaterials.

Introduction

Cancer has been a major leading cause of human death over decades.[1] Various cancer treatments have been developed such as surgery, chemotherapy, radiotherapy, immunotherapy, and so on, but still challenges are faced such as side effects and recurrences.[2,3] The emergence of nanotechnology has provided various nanoplatforms with multiple therapeutic modalities integrated in a synergistic way for more efficient therapy.[4,5] Porous hollow inorganic nanomaterials with intrinsic therapeutic functionalities have attracted much attention as delivery systems for therapeutic agents.[6,7] Mesoporous silica nanoparticles (NPs) are well-known delivery systems with finely tuned porosity for multi-drug loading.[8,9] However, the control of the drug release is majorly dependent on the functionality of their surface coating.[10,11] Porous hollow gold or palladium NPs with intrinsic photothermal capability have also been used as drug carriers.[12,13] The heat generated upon laser irradiation not only could accelerate the drug release in a more controllable manner, but also showed synergism with chemotherapy.[14] Nevertheless, the nonbiodegradability of noble metals raised concerns about their long-term biosafety.[15] Porous hollow CuS NPs with not only efficient heat generation

ability, but also excellent biodegradability are more favorable.[16] But, the current template-assisted synthesis method could not guarantee a uniform morphology and the product is usually over one hundred nanometres in size.

Galvanic replacement reactions provide a powerful tool to synthesize noble metal or metal oxide hollow nanostructures.[17,18] Seed-mediated growth in organic solvents allows precise control of the size, shape, and composition of nanocrystals.[19] Here, we synthesized around 14 nm porous hollow copper iron oxide nanoparticles (PHCuFeNPs) with 2–3 nm pores *via* the galvanic reaction between Cu_2S NPs and iron pentacarbonyl ($Fe(CO)_5$) followed by etching at high temperature to make pores. We previously reported porous hollow iron oxide nanoparticles,[20,21] which were able to load cisplatin drugs and stay stable under normal physiological conditions after surface modification with polyethylene glycol, but resulting in accelerated cisplatin release in a weak acidic tumor microenvironment due to the pore etching. Similarly, these PHCuFeNPs also demonstrated a pH-responsive drug release behaviour but were more sensitive to weak acids due to their unstable copper valence and more defective crystals created during the galvanic reaction. The copper release was up to 37.9% and could effectively catalyze the reaction of hydrogen peroxide to produce hydroxyl radicals (·OH) for chemodynamic therapy. Besides, the PHCuFeNPs retained the absorption in the near-infrared region and could effectively heat up upon 980 nm laser irradiation. We also observed immunogenic cell death (ICD) induced by PHCuFeNPs to activate the immune system. Therefore, we believe that these PHCuFeNPs could combine multi-antitumor therapeutic approaches in a synergistic way (Scheme 1). Their ability to degrade into fragments for fast renal clearance also guarantees biosafety.

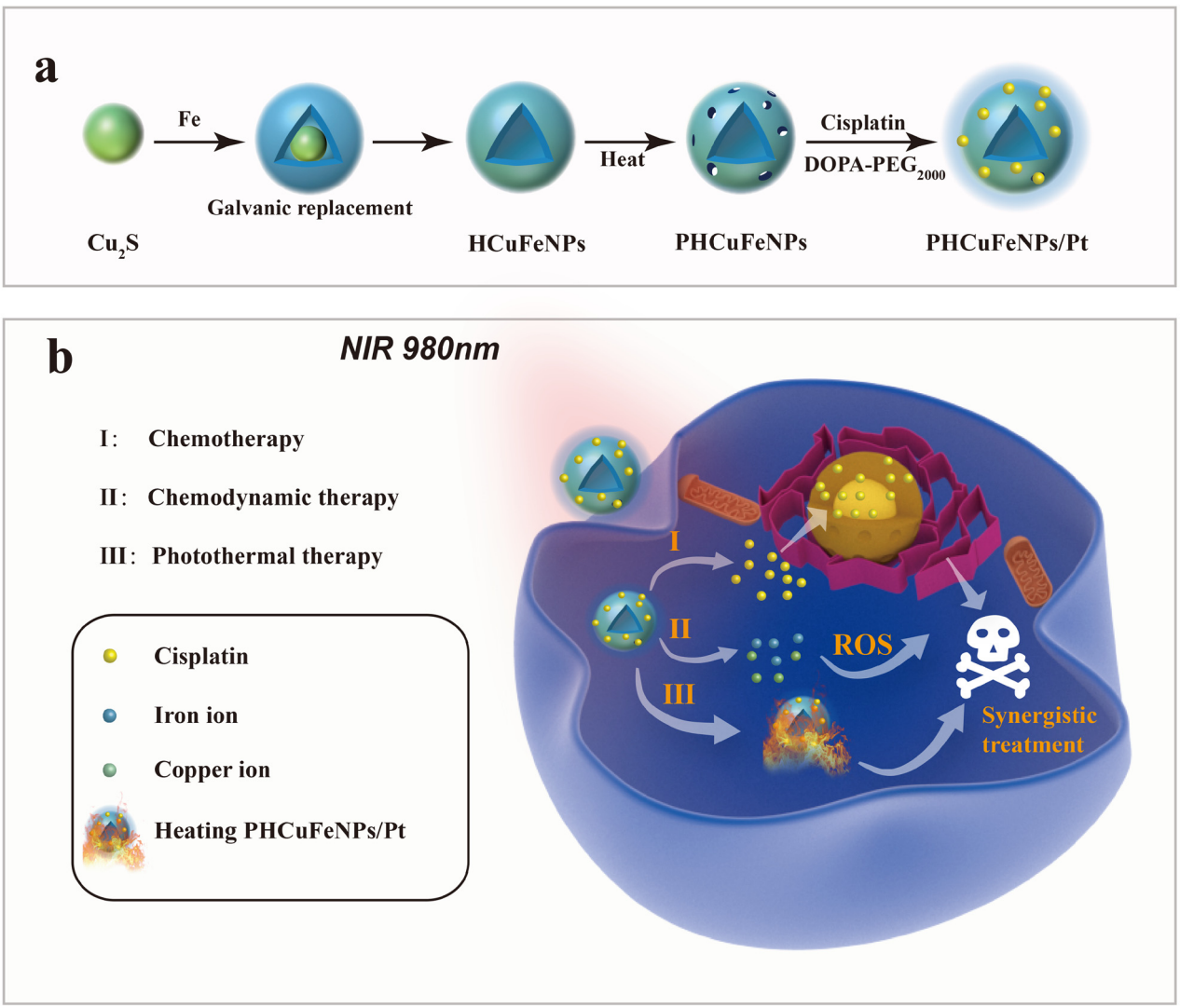

Scheme 1 (a) Schematic illustration of the preparation of cisplatin-loaded PHCuFeNPs (PHCuFeNPs/Pt). (b) The proposed trimodal chemo-, chemodynamic-, photothermal anti-tumor therapy based on PHCuFeNPs/Pt.

Experimental section

Materials

Copper(II) chloride dihydrate ($CuCl_2{\cdot}2H_2O$), sulfur (S), ammonium bromide (NH_4Br), iron pentacarbonyl ($Fe(CO)_5$), 1-octadecene (ODE, 90%), oleylamine (OAm, 70%), oleic acid (OA, 70%), benzyl ether (BE, 98%), cisplatin and 4,4′-diamino-3,3′,5,5′-tetramethyl biphenyl (TMB) were purchased from Sigma-Aldrich. Cy7 dye was purchased from RuixiBio Tech. 2′,7′-Dichlorodihydrofluorescein diacetate (DCFH-DA), 3-(4,5-dimethylthiazol-2-yl)-2,5-diphenyltetrazolium bromide (MTT), RPMI 1640 medium, and trypsin were purchased from KeyGen Biotech. Calreticulin antibody was purchased from Proteintech Group, Inc. IFN-γ, IL-6, and TNF-α enzyme-linked immunosorbent assay (ELISA) kits were purchased from Cloud-clone corp.

The transmission electron microscopy (TEM) images were obtained on a JEOL JEM-2100f. The hydrodynamic size was measured using a Malvern Zetasizer Nano ZS90. The X-ray diffraction pattern was recorded using the ARL XTRA diffractometer. X-ray photoelectron spectroscopy (XPS) was performed using the Kratos Model Axis Supra system. The concentration of each element was determined by inductively coupled plasma optical emission spectrometry (ICP-OES, Agilent 700 Series).

Synthesis of PHCuFeNPs

Cu_2S NPs were synthesized by a previously reported method.[22] Briefly, $CuCl_2$ which was dissolved in 30 mL of octadecene and 5 mL of oleylamine was reacted with a sulfur solution in the presence of 5 mL of octadecene. After being maintained at 120 °C for 1 h, 0.05 mmol sulfur solution was injected and quickly heated to 180 °C for another 1 h. The as-prepared Cu_2S NPs were purified by centrifugation.

To synthesize hollow copper iron oxide nanoparticles (HCuFeNPs), 30 mg of Cu_2S NPs were mixed with 8 mg of ammonium bromide, 10 mL of octadecene, and 0.3 mL of oleylamine. After being maintained at 120 °C for 1 h, 0.1 mL of $Fe(CO)_5$ was injected quickly and the system was further heated to 180 °C at a rate of 1 °C min^{-1}. The solution was maintained at this temperature for an additional 30 min before it was cooled down to room temperature. The as-synthetic HCuFeNPs were precipitated with ethanol and purified by centrifugation.

The pore-opening process followed a reported method.[20] Briefly, 30 mg of HCuFeNPs were mixed with dibenzyl ether in the presence of oleylamine and oleic acid before being heated to 120 °C and maintained for 0.5 h. Then, the system was heated to 260 °C for another 1 h. The product was washed with ethanol and purified by centrifugation.

Preparation of cisplatin-loaded PHCuFeNPs

The drug loading process was reported before.[20] Briefly, 20 mg of PHCuFeNPs and 6 mg of cisplatin were dispersed in a mixture of chloroform and *N*,*N*-dimethylformamide (DMF) before 60 mg of DOPA–PEG_{2000} was added. After overnight stirring and vacuum drying, cisplatin-loaded PHCuFeNPs (PHCuFeNPs/Pt) were dispersed in water and purified using PD-10 columns.

Photothermal measurements

To examine the photothermal properties of PHCuFeNPs, different concentrations of NPs (12.5, 25, 50 and 100 μg mL^{-1}) were irradiated with a 980 nm laser at different powers (1–2 W cm^{-2}), and the temperature was recorded using an infrared thermal imager (FLUKE Ti400, USA) every 20 s. The thermal stability was tested by repeatedly irradiating the samples five times.

Cu, Fe and Pt drug release measurements

Cu_2S, HCuFeNPs, PHCuFeNPs and PHCuFeNPs/Pt (2 mg mL^{-1} Cu, 1 mL) were respectively added into a dialysis bag (MCWO: 500 Da) and immersed in a 50 mL centrifuge tube filled with 20 mL of PBS (pH 7.4 or pH 5.5). 1 mL of PBS was taken at different time points and replaced with 1 mL of fresh PBS. The concentrations of Cu, Fe, and Pt were detected by ICP-OES.

Hydroxyl radical generation measurement

The TMB assay was used to evaluate the ·OH generation. Briefly, 100 μg mL^{-1} nanoparticles, 200 μg mL^{-1} TMB, and 80 mM H_2O_2 were mixed in PBS buffer (pH 7.4 or pH 5.5) at 37 °C for 15 min, and then the absorbance from 350 to 800 nm was measured using an ultraviolet spectrophotometer (Multiskan Sky, Thermo Fisher Scientific).

In vitro cytotoxicity assay and intracellular ROS measurement

Murine mammary carcinoma cells (4T1) and human normal liver cells (L02) were seeded in 96-well plates (1×10^4 cells per well) for 24 h. Then, the cells were respectively treated with Cu_2S, PHCuFeNPs, or PHCuFeNPs/Pt at different concentrations (3.13, 6.25, 12.5, 25, 50 and 100 μg mL^{-1}) for 18 h before either with or without irradiation with a 980 nm laser (1.5 W cm^{-2}) for 10 min. After incubation for another 6 h, the cell viability was tested by the MTT assay.

For the intracellular ROS measurement, 4T1 cells were seeded in 6-well plates. A 980 nm laser was used to irradiate the cells with PHCuFeNPs, or PHCuFeNPs/Pt (20 μg mL^{-1}) for 10 min, and the cells were incubated for another 6 h and stained with 10 μM DCFH-DA for 20 min. After being washed with PBS, the cellular images were recorded by fluorescence microscopy.

In vitro detection of calreticulin (CRT) expression

The cells were then labeled with the Alexa Fluor 488-CRT antibody and the nuclei were stained with DAPI. Finally, the cells were washed with PBS twice and the fluorescence was recorded by fluorescence microscopy.

In vivo antitumor experiments

Balb/c mice (female, 4–5 weeks old) were purchased from Qinglongshan (Nanjing, China). Animal procedures were performed according to the Guidelines for Care and Use of Laboratory Animals in research of China Pharmaceutical University and approved by the Ethics Committee of China

Pharmaceutical University. The 4T1 tumor-bearing mice were established by injecting subcutaneously 2×10^6 4T1 cells into the right hind legs. When the tumors reached 100 mm^3, the mice were randomly divided into five groups: (a) PBS group, (b) PHCuFeNPs group, (c) PHCuFeNPs/Pt group, (d) PHCuFeNPs + laser group, and (e) PHCuFeNPs/Pt + laser group. The PHCuFeNPs or PHCuFeNPs/Pt (250 μg kg^{-1} Cu) were injected intratumorally before being irradiated with a 980 nm laser (1.5 W cm^{-2}) for 10 min. The tumor volume was calculated according to the formula: volume = (length × $width^2$/2). Seven days after different treatments, the mouse serum was collected to determine the content of IFN-γ, TNF-α, and IL-6 using an ELISA kit. The tumor sections were collected for immunological assessment. Fourteen days after treatments, the tumor sections were collected for hematoxylin/eosin (H&E) and the terminal dUTP-mediated nick-end-labeling (TUNEL) staining.

In vivo biodistribution and biosafety studies

To trace the biodistribution of PHCuFeNPs, the near-infrared fluorescence dye sulfo Cy7-NHS was conjugated onto PHCuFeNPs *via* reacting with the dopamine–PEG_{2000}–NH_2. After intratumoral injection, the fluorescence signal was detected at different time points using a fluorescent biological image analysis system, Tanon 4600SF (Tianneng, China). The urine was collected at different time points for copper quantification *via* ICP-OES.

To determine the biosafety of PHCuFeNPs/Pt, the blood of mice after treatment was collected for blood routine tests and blood biochemistry tests at Servicebio Company. The major organs (the heart, liver, spleen, lungs and kidneys) were collected for H&E staining.

Statistical analysis

All data were expressed as the mean ± standard deviation (SD). One-way ANOVA was used for the statistical analysis using Graphpad prism 9, and p-value < 0.05 (*P < 0.05, **P < 0.01, ***P < 0.001) was considered statistically significant.

Results and discussion

Synthesis and characterization of porous hollow copper iron oxide nanoparticles

The hollow copper iron oxide nanoparticles (HCuFeNPs) were prepared *via* the galvanic reaction between Cu_2S NPs and $Fe(CO)_5$. The solid spherical Cu_2S NPs with a uniform size of around 12 nm were synthesized following a previously reported method (Fig. 1a).[22] Upon adding 0.05 mL of $Fe(CO)_5$, small

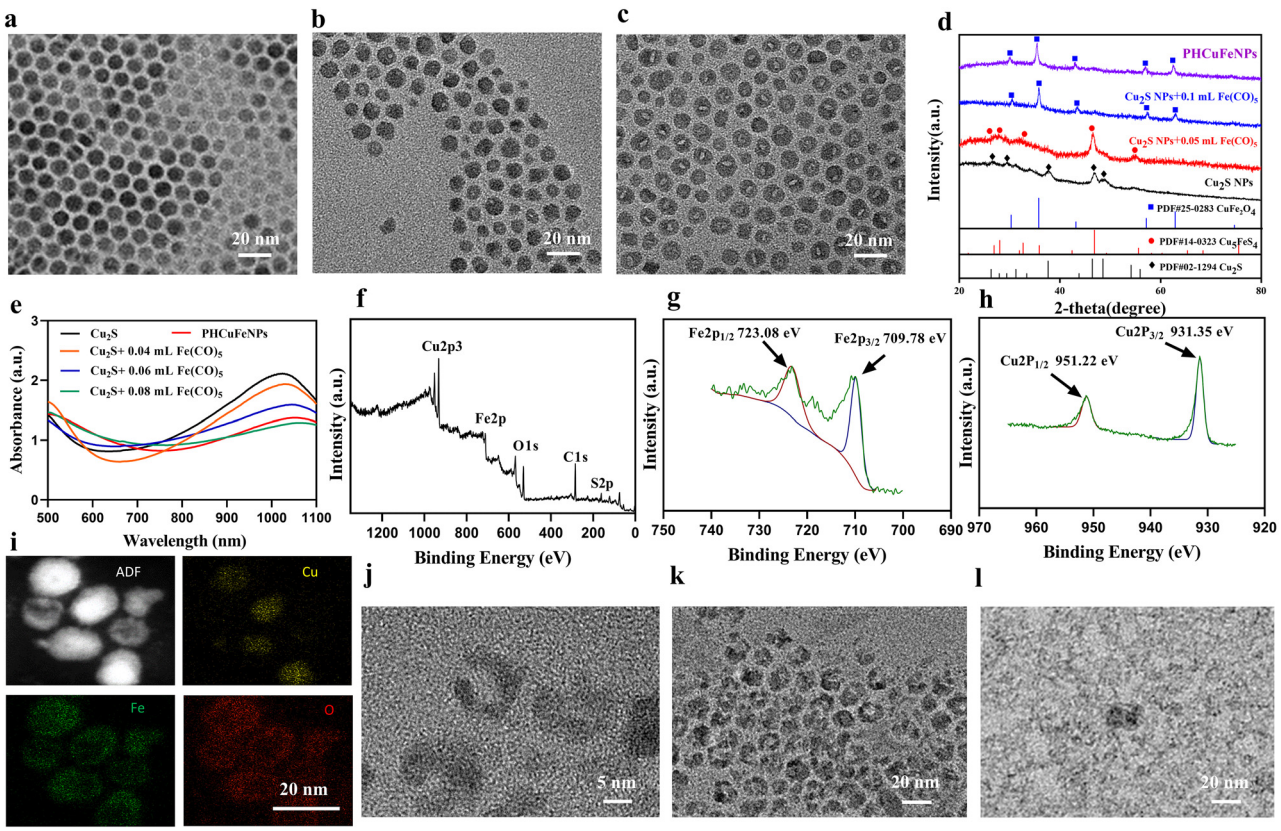

Fig. 1 (a–c) TEM images of Cu_2S before (a) and after the reaction with 0.05 mL $Fe(CO)_5$ (b) and 0.1 mL $Fe(CO)_5$ (c). Scale bar: 20 nm. (d) XRD patterns of Cu_2S, Cu_2S reacted with 0.05 mL and 0.1 mL $Fe(CO)_5$ and PHCuFeNPs. (e) UV absorption spectra of Cu_2S, Cu_2S reacted with 0.04 mL, 0.06 mL and 0.08 mL $Fe(CO)_5$ and PHCuFeNPs. (f–h) XPS of HCuFeNPs. (i) STEM-EDS mapping of PHCuFeNPs. Scale bar: 20 nm. (j) TEM images of PHCuFeNPs. Scale bar: 5 nm. (k–l) TEM images of PHCuFeNPs incubated at pH 7.4 (k) and pH 5.5 (l) at 37 °C for 8 h. Scale bar: 20 nm.

voids could be observed in some NPs as shown in Fig. 1b. Continuous addition of $Fe(CO)_5$ led to larger voids and almost all the NPs showed hollow structures when 0.1 mL of $Fe(CO)_5$ was added (Fig. 1c). The asymmetric voids indicated that the etching started from one side, which is consistent with the previous report.[23] The X-ray diffraction (XRD) pattern demonstrated the presence of the Cu_5FeS_4 phase upon subjecting Cu_2S to a small amount of $Fe(CO)_5$, which was further converted to the $CuFe_2O_4$ phase when a complete hollow structure was observed upon subjecting it to a large amount of $Fe(CO)_5$ (Fig. 1d). The UV-vis spectrum was also obtained to study the reaction process (Fig. 1e). Upon gradual addition of $Fe(CO)_5$, the absorption peak of Cu_2S at around 1000 nm was decreased correspondingly, which further confirmed the gradual crystal phase conversion. X-ray photoelectron spectroscopy (XPS) was also used to study the composition of complete hollow NPs. As shown in Fig. 1f–h, the binding energy (EB) values for Cu (2p) showed two peaks at around 931.35 eV and 951.22 eV, corresponding to the orbitals of Cu $2p_{3/2}$ and Cu $2p_{1/2}$, and no satellite peaks were detected (Fig. 1h), indicating that copper was in the Cu(I) or Cu(0) valence. The Fe 2p spectrum also showed two peaks at 709.78 eV and 723.08 eV, corresponding to the orbitals of Fe $2p_{3/2}$ and Fe $2p_{1/2}$, indicating a mixture of Fe(II) and Fe(III) (Fig. 1g). A small peak of S (Fig. 1f) was also observed, indicating that the HCuFeNPs might not be completely converted, but with the $CuFe_2O_4$ phase dominating.

The PHCuFeNPs were then obtained by heating HCuFeNPs rapidly to 260 °C in the presence of oleic acid. This strategy has been reported before to make pores on hollow iron oxide structures.[20] It is believed that the uneven growth of the crystal domain in the shell structure could lead to the formation of porous shells. As shown in Fig. 1j, the PHCuFeNPs had a cavity of around 5–6 nm in diameter, an uneven shell and around 2 nm pores in the shell. The XRD pattern (Fig. S1b†) and XPS (Fig. S2a–c†) results confirmed that the pore-opening process did not change the crystal phase with the characteristic peaks similar to that of HCuFeNPs (Fig. 1f–h and Fig. S1a†). The STEM-energy dispersive (EDS) elemental mapping of PHCuFeNPs is shown in Fig. 1i, with a uniform distribution of Cu, Fe and O around the NPs. The UV absorption of PHCuFeNPs still demonstrated a small peak at around 1000 nm (Fig. 1e), indicating the possibility for near-infrared light-induced photothermal therapy. The as-prepared PHCuFeNPs were coated with oleylamine/oleic acid which is hydrophobic. After replacing the original ligand with dopamine–polyethylene glycol (DOPA–PEG), they became water dispersible with a hydrodynamic size of around 21 nm (Fig. S3†). The modified PHCuFeNPs stayed integrated with no obvious morphology change after incubation at pH 7.4 (Fig. 1j and k), but were sensitive to acid etching and completely cracked after incubation at pH 5.5 for 8 h (Fig. 1l).

In vitro photothermal properties, controlled drug release and ROS production

The PHCuFeNPs demonstrated a concentration- (Fig. 2a) and laser power- (Fig. 2b) dependent temperature increase upon 980 nm laser irradiation. As shown in Fig. 2a, after irradiating at 1.5 W cm^{-2} for 10 min, the temperature of PHCuFeNPs quickly increased to over 70 °C at a concentration of 100 μg mL^{-1}, which is more effective than Cu_2S NPs (to 65 °C, Fig. S4a†) at the same concentration of Cu, probably due to the additional iron component. Besides, the temperature increase of PHCuFeNPs did not change significantly during the five hot-cold cycles (Fig. S4b†), indicating their excellent photothermal stability.

We then investigated the drug delivery capability of PHCuFeNPs. We used cisplatin, a clinical anticancer drug with poor water solubility, as a model and followed a reported method.[20] Briefly, cisplatin was first mixed with PHCuFeNPs in the organic phase and then loaded into the cavity upon a concentration gradient created by evaporation, before being wrapped by the dopamine–PEG_{2000} polymer, to produce PHCuFeNPs/Pt. The loading efficiency is calculated to be 32.68% as measured by inductively coupled plasma atomic emission spectrometry (ICP-OES).

The Fe ions, Cu ions and Pt release were then monitored at different pH values. As shown in Fig. S5,† Cu_2S NPs release copper ions of about 9.37% at pH 5.5. In comparison, the release of copper from PHCuFeNPs was around 12% at pH 7.4 and significantly increased to 21.27% at pH 5.5 within 24 h (Fig. 2c). The Fe ion release was also increased from 4.18% at pH 7.4 to 7.63% at pH 5.5 (Fig. 2d). It is worth mentioning that porous hollow iron oxide nanoparticles (PHIONPs) with a similar size also demonstrated a slight increase of iron release (3.1%) at pH 5.5 compared to that (1.6%) at pH 7.4 due to the acidic etching induced degradation.[21] We assumed that when the PHCuFeNPs went through a similar etching process, the galvanic reaction between Fe(0) and Cu_2S provided an unstable copper valence and more defective crystal structures, which made Fe and Cu more sensitive to pH. We also observed an accelerated cisplatin release at pH 5.5 due to the pore etching process (Fig. 2e). What's more, the heat generated by the external laser application further promoted the etching process and release of cisplatin. A sudden increase in release of Fe, Cu and Pt was observed upon laser irradiation (980 nm, 1.5 W cm^{-2}) for 5 min (Fig. 2c–e). It is worth mentioning that the following second and third laser irradiation did not cause a burst release as the first time did. It might be because the heat generated during the first laser irradiation already caused nanoparticles to crack.

Copper and iron ions are well-known catalytically active ions in the Fenton reaction to decompose hydrogen peroxide (H_2O_2) into ·OH.[24–26] We then tested the reactive oxygen species (ROS) production of PHCuFeNPs *via* the 3,3′,5,5-tetramethylbenzidine (TMB) assay. As shown in Fig. 2f, in the presence of H_2O_2, Cu_2S NPs could barely change the TMB colour, while PHCuFeNPs significantly increased the absorption at 652 nm, indicating the production of ROS. The higher catalytic activity of PHCuFeNPs was observed at pH 5.5 than that at pH 7.4, confirming their catalytic selectivity in a weak acidic microenvironment.

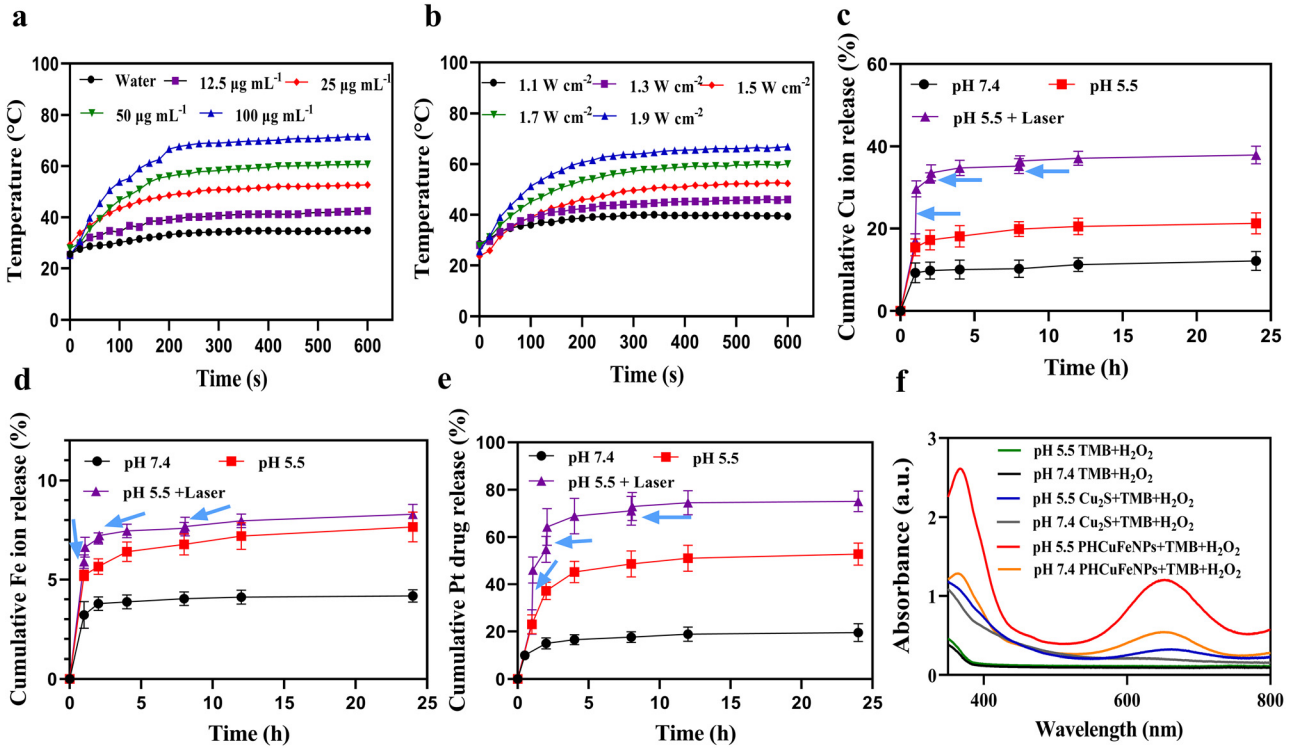

Fig. 2 (a) The temperature increase curves of PHCuFeNPs at different concentrations (0, 12.5, 25, 50 and 100 μg mL^{-1}) upon laser irradiation (980 nm, 1.5 W cm^{-2}) for 10 min. (b) The temperatures of PHCuFeNPs at 25 μg mL^{-1} under laser irradiation with different powers (1.1, 1.3, 1.5, 1.7, 1.9 W cm^{-2}). (c–e) Cu ion (c), Fe ion (d) and cisplatin (e) release from PHCuFeNPs/Pt at pH 7.4, pH 5.5 and pH 5.5 under 980 nm laser irradiation. Arrow: irradiated. Data represent mean ± SD, n = 3. (f) UV/vis absorption of 3,3′,5,5′-tetramethylbenzidine (TMB) solution after mixing with Cu_2S and PHCuFeNPs in 15 min.

In vitro anti-tumor experiments

The synergistic therapeutic effect of PHCuFeNPs/Pt was then studied on 4T1 cells. Copper and iron ions are known to be toxic to cells at high concentrations.[27,28] Cu_2S NPs which had negligible copper release showed excellent biocompatibility with nearly all the cells viable after being treated with a concentration of up to 100 μg mL^{-1} copper for 24 h (Fig. 3a). In comparison, the PHCuFeNPs showed obvious dose-dependent cytotoxicity in 4T1 cells with over 43% killed at a concentration of 100 μg mL^{-1} Cu. Since the PHCuFeNPs showed a similar iron release to that of PHIONPs, and we previously proved that PHIONPs killed no cells at a concentration of 100 μg mL^{-1} Fe,[21] we assumed that the toxicity was mainly ascribed to copper. It is worth mentioning that like many other NPs with Fenton catalytic activity, the PHCuFeNPs demonstrated intrinsic selectivity between tumor cells and normal cells. The half maximal inhibitory concentration (IC_{50}) of PHCuFeNPs in 4T1 cells was around 50 μg mL^{-1} Cu and 28 μg mL^{-1} Fe, which was much lower than that in normal liver cells L02 (Fig. 3b).

The PHCuFeNPs/Pt + laser treatment demonstrated a synergistic therapeutic effect of chemodynamic therapy, photothermal therapy and chemotherapy (Fig. 3c). As shown in Fig. 3a, when the cell viability reached 43.98% after being treated with PHCuFeNPs for chemodynamic therapy, the cell viability was down to 27% after being treated with PHCuFeNPs/Pt (Cu: 100 μg mL^{-1}, Fe: 56 μg mL^{-1}, cisplatin: 29 μg mL^{-1}) with the help of cisplatin chemotherapy. Laser irradiation (980 nm, 1.5 W cm^{-2}, 10 min) further enhanced the anticancer effect with only 9.09% cell viability after treatment with PHCuFeNPs/Pt + laser.

We then investigated the ROS production level in 4T1 cells after different treatments using the 2′,7′-dichlorofluorescein diacetate (DCFH-DA) probes.[29] After cellular uptake, DCFH-DA was acetylated and reacted with ROS to produce green fluorescence. As shown in Fig. 3d and f, the cell treated with PHCuFeNPs showed enhanced green fluorescence compared with that treated with PBS, confirming their chemodynamic activity. Delivering cisplatin or heating by irradiation could further promote the ROS level. The cells treated with PHCuFeNPs/Pt + laser demonstrated the highest green fluorescence, confirming that integrating CDT, PTT and chemotherapy could produce more ROS in a synergistic way.

It is generally known that ROS can induce immunogenic cell death (ICD) which could further activate the immune system to fight cancer.[30,31] We then investigated the ICD induced by different treatments by measuring the calreticulin (CRT) expression. CRT is a widely used indicator of ICD and is transferred to the surface of the tumor cell membrane from the endoplasmic reticulum during ICD. As shown in Fig. 3e

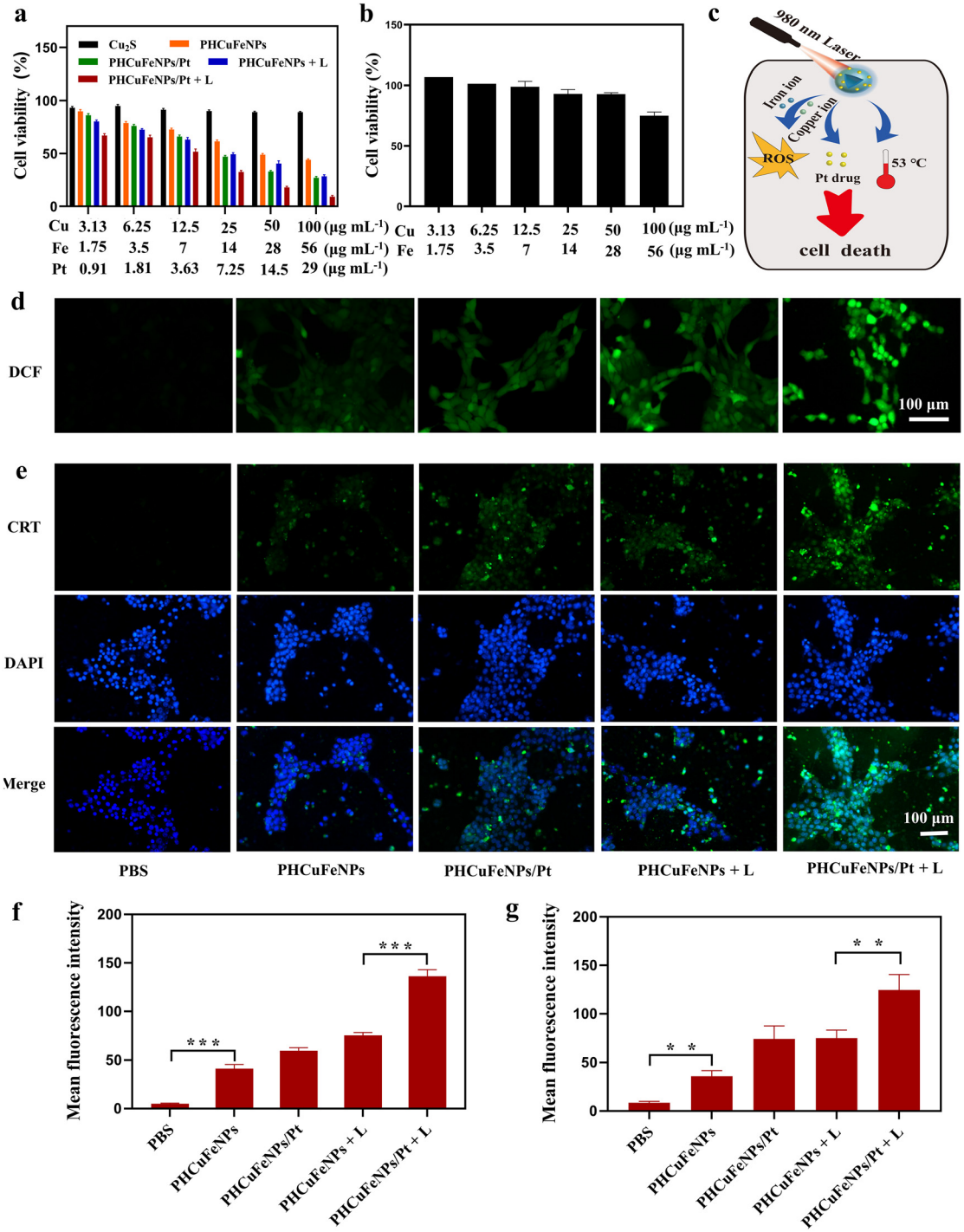

Fig. 3 (a) Cell viability of 4T1 cells after different treatments for 24 h. Groups: Cu_2S NPs, PHCuFeNPs, PHCuFeNPs/Pt, PHCuFeNPs + laser and PHCuFeNPs/Pt + laser. (b) Cell viability of L02 cells after being treated with PHCuFeNPs. (c) The schematic diagram of the synergistic killing of tumor cells by PHCuFeNPs/Pt + laser. (d) Fluorescence imaging of 4T1 cells stained with DCFH-DA after 6 h with or without 980 nm laser irradiation, and (f) the corresponding pixel intensity of green fluorescence, indicating the ROS level. Scale bar: 100 μm. (e) Immunofluorescence images of 4T1 cells labeled with the Alexa-488-anti-CRT antibody after different treatments and (g) the corresponding pixel intensity of green fluorescence, indicating the CRT expression. Scale bar: 100 μm. Data represent mean ± SD, $n = 3$. $^{**}P$ value < 0.01, $^{***}P$ value < 0.001.

and g, the CRT expression after being treated with PHCuFeNPs/Pt + laser was 3.45 times higher than that treated with PHCuFeNPs only, 1.67 times higher than that treated with PHCuFeNPs/Pt, and 1.65 times higher than that treated with PHCuFeNPs + laser. Overall, we believed that the PHCuFeNPs could serve as a cisplatin delivery system, a copper

and iron ion source and a photothermal agent to significantly promote ROS production to kill cancer cells and induce ICD for potential immunotherapy.

In vivo anti-tumor effect

We then studied the *in vivo* therapeutic effectiveness of PHCuFeNPs/Pt for chemodynamic-, photothermal- and chemo-trimodal anti-cancer therapy in 4T1 tumor-bearing mice. When the tumor grew to 100 mm^2, the mice were divided randomly into five groups: (1) PBS, (2) PHCuFeNPs, (3) PHCuFeNPs/Pt, (4) PHCuFeNPs + laser, and (5) PHCuFeNPs/Pt + laser. We injected the nanoplatforms (Cu, 5 μg; Fe, 2.8 μg; Pt, 1.45 μg) intratumorally to make sure a better control of NPs dosage for comparison.

The local tumor region was then irradiated with a 980 nm laser (1.5 W cm^{-2}, 10 min). As monitored using a infrared (IR) thermal camera (Fig. 4a), the temperature of the tumor injected with PHCuFeNPs or PHCuFeNPs/Pt had dramatically increased to over 53 °C; when the tumor was treated with PBS, the temperature only slightly rose to 41 °C, indicating the *in vivo* photothermal effect of PHCuFeNPs (Fig. 4b). The tumor growth was monitored within 24 days (Fig. 4c and d).

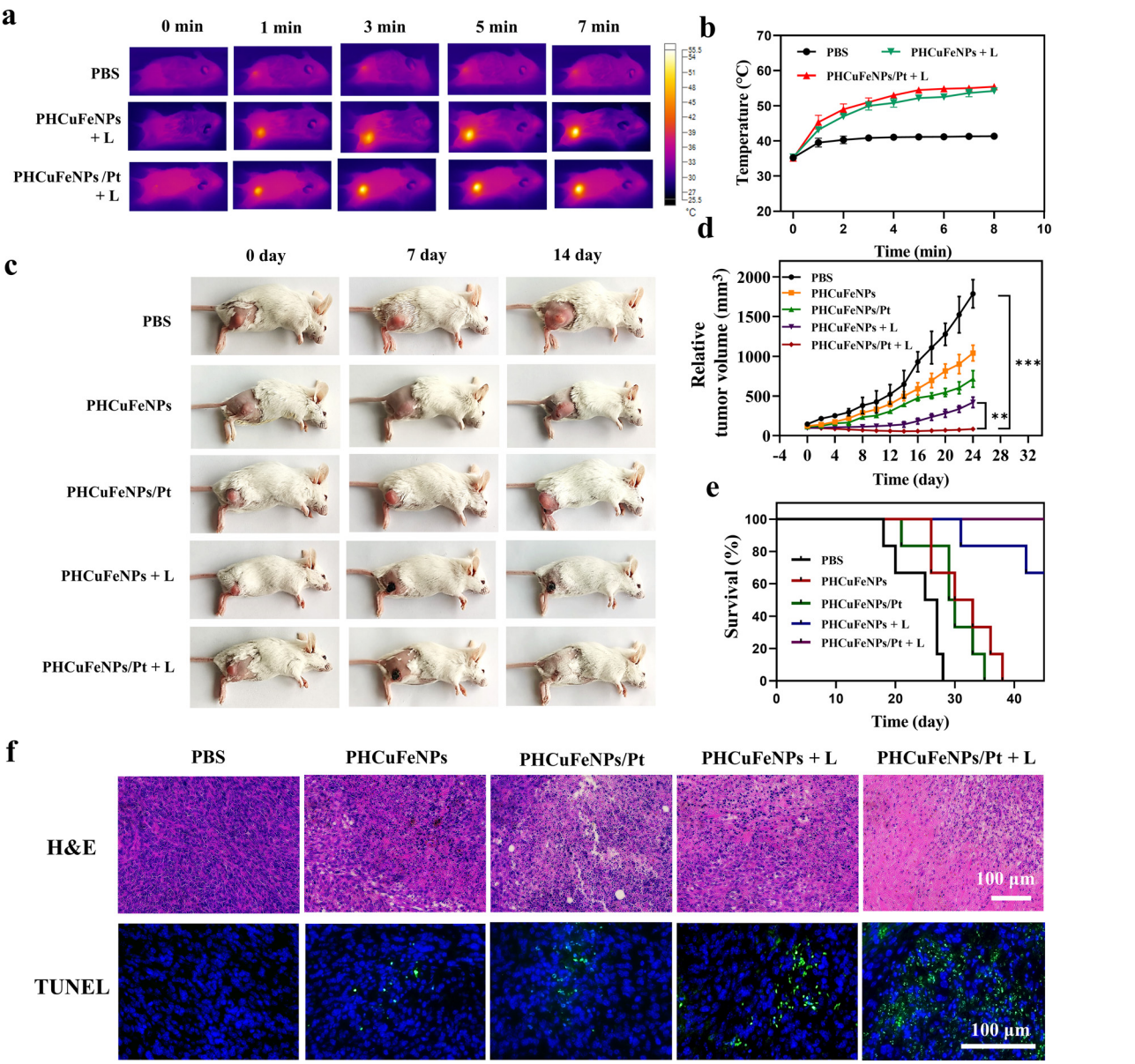

Fig. 4 (a–b) Photothermal images (a) and the corresponding temperature changes (b) at different points under 980 nm laser irradiation (1.5 W cm^{-2}, 10 min). Data represent mean ± SD, n = 3. (c) The pictures of mice on the 0th, 7th and 14th day after different treatments. (d–e) Relative tumor volumes (d) and survival curves (e) after different treatments (n = 6). (f) H&E and TUNEL staining of tumors 14 days after different treatments. Scale bar: 100 μm. **P value < 0.01, ***P value < 0.001.

Compared with the PBS group, the groups treated with PHCuFeNPs showed some delay in tumor growth, indicating the intrinsic anti-tumor capability of PHCuFeNPs. Combination of both cisplatin delivery and laser irradiation improved the therapeutic effect to some extent, while the groups treated with PHCuFeNPs/Pt + laser completely suppressed the tumor. What's more, no tumor reoccurrence or mouse death was observed in the PHCuFeNPs/Pt + laser group within 40 days (Fig. 4e). Meanwhile, no significant body weight change was observed after the treatments (Fig. S6†). The anti-tumor effect was also confirmed by hematoxylin–eosin (H&E) staining and terminal dUTP-mediated nick-end-labeling (TUNEL) staining. As shown in Fig. 4f, the tumor treated with PHCuFeNPs/Pt + laser had the most necrotic and apoptotic cells 14 days after the treatment.

Based on the *in vitro* result that PHCuFeNPs/Pt + laser treatment could significantly induce ICD, we also evaluated its ability to enhance tumor T cell infiltration *in vivo*. The immunofluorescence staining results showed much higher populations of $CD4^+$ and $CD8^+$ T cells in the tumor after PHCuFeNPs/Pt + laser treatment than those after all the other treatments (Fig. 5a). Moreover, we also detected IL-6, TNF-α and IFN-γ which are important cytokines secreted by activated T cells in serum *via* ELISA. As shown in Fig. 5b, when only PHCuFeNPs, PHCuFeNPs/Pt and PHCuFeNPs + laser treatment all increased these cytokines to some extent, the PHCuFeNPs/Pt + laser treatment showed the highest immune response with 1.5-fold IFN-γ and TNF-α higher and 7-fold IL-6 higher than that of the PBS group. All these results indicate that PHCuFeNPs/Pt + laser could significantly activate the immune response and could potentially combine with immunotherapy.

The biosafety of PHCuFeNPs

The long-term toxicity of nanoparticles is a major concern for their potential clinical use.[32] Renal clearable nanocarriers with an enhanced body elimination ability have attracted much attention recently. Our PHCuFeNPs were already proved to be unstable in a weak acidic microenvironment and could be disintegrated into fragments (<8 nm) possible for renal clearance (Fig. 1l). We then conjugated them with Cy7 dye and studied their *in vivo* biodistribution by near-infrared fluorescence imaging. As shown in Fig. 6a, an obvious fluorescence signal appeared in the bladder 30 min after laser irradiation. We also collected urine to quantify the copper amount by ICP-OES. The copper concentration in the urine was the highest within 4 h and gradually reduced over time (Fig. 6b), consistent with the fluorescence imaging results, which indicated that PHCuFeNPs could be metabolized into the urine rapidly. It is worth mentioning that without laser irradiation, the PHCuFeNPs were eliminated *via* urine much slower (Fig. S7†). We believed that laser irradiation greatly accelerated the degra-

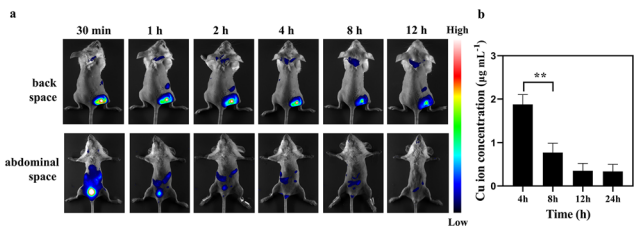

Fig. 6 (a) *In vivo* mouse imaging after treatment with PHCuFeNPs–Cy7 and (b) Cu ion concentrations in urine under 980 nm laser irradiation (1.5 W cm^{-2}, 10 min). Data represent mean ± SD, n = 3. $^{**}P$ value < 0.01.

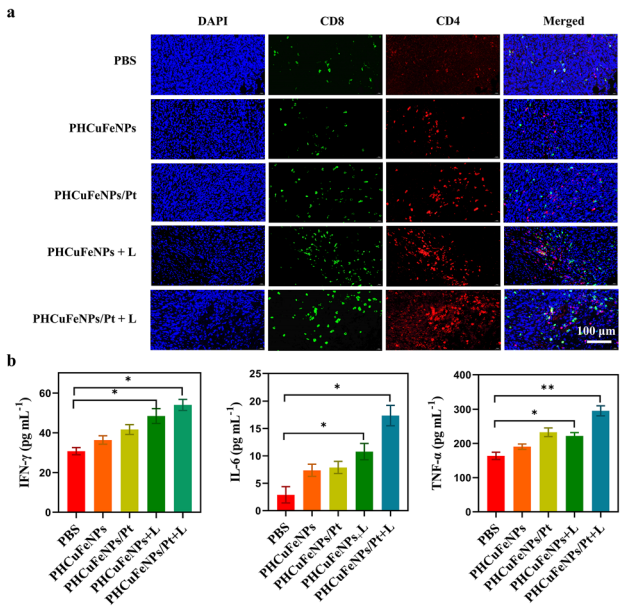

Fig. 5 (a) Immunofluorescence staining of $CD4^+$ T cells and $CD8^+$ T cells in the tumor tissue section. Scale bar: 100 μm. (b) Quantification of TNF-α, IL-6 and IFN-γ in serum seven days after different treatments. Data represent mean ± SD, n = 3. $^{*}P$ value < 0.05, $^{**}P$ value < 0.01.

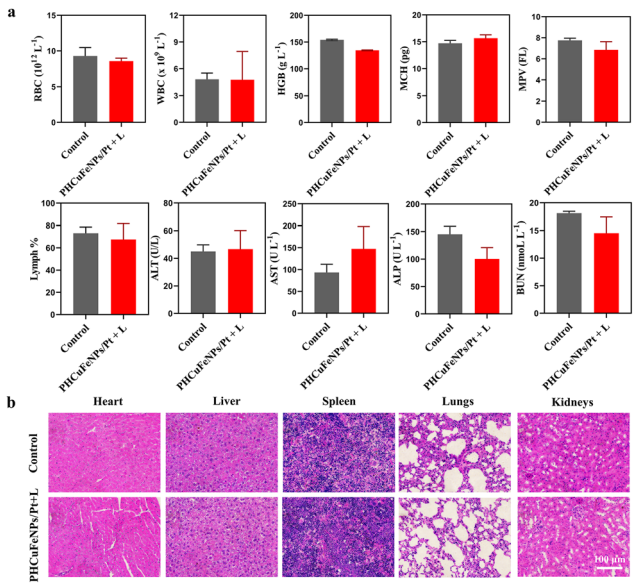

Fig. 7 (a) The blood routines and blood biochemistry of healthy mice without or with PHCuFeNPs/Pt + laser treatment. Data represent mean ± SD, n = 3. (b) The H&E staining of the major organs (the heart, liver, spleen, lungs and kidneys) after treatment. Scale bar: 100 μm.

dation of PHCuFeNPs, resulting in fast renal clearance. To further evaluate the biosafety of PHCuFeNPs/Pt, the mouse blood samples were collected one day after the treatment for blood routine and blood biochemistry tests (Fig. 7a). All the indexes were within the normal range. Besides, the H&E staining of the major organs (the heart, liver, spleen, lungs and kidneys) was conducted on the 14th day post-injection (Fig. 7b) with no inflammatory response observed. Thus, we believe that the PHCuFeNPs have excellent biocompatibility.

Conclusion

In summary, we synthesized around 14 nm PHCuFeNPs with 5–6 nm cavities and 2–3 nm pore sizes that could serve not only as a photothermal agent, but also as a drug carrier. The pores of PHCuFeNPs etched in a weak acidic tumor microenvironment enabled controlled Cu and Fe ion release, which could drive the Fenton reaction to accomplish CDT and accelerate the cisplatin release to achieve chemotherapy. Upon laser irradiation, the heat generated by PHCuFeNPs not only realized effectively PTT, but also stimulated the release process. The synergizing CDT, PTT and chemotherapy could effectively inhibit the growth of tumor cells *in vitro* and *in vivo*. Besides, the ICD induced by PHCuFeNPs could activate the T cell-mediated immune system and achieve complete tumor elimination by combining with multi-antitumor therapy. Accompanied by the rapid renal clearance capacity, these PHCuFeNPs integrating CDT, PTT, and chemotherapy could be a promising biocompatible and efficient strategy against cancer.

Author contributions

Kai Feng: investigation, data curation, visualization, and writing – original draft. Zhengtao Xu: data curation, visualization, and writing – original draft. Yuhan Wang: visualization, investigation and editing. Xiyao Wu: visualization and investigation. Fucheng Xiong: visualization and investigation. Yiling Ruan: visualization and editing. Xiaojing Wu: visualization and investigation. Linqian Ye: visualization. Dong Su: validation, supervision, and writing – reviewing. Jing Yu: validation, supervision, writing – reviewing and funding acquisition. Xiaolian Sun: conceptualization, validation, supervision, writing – reviewing and editing, funding acquisition, and project administration.

Conflicts of interest

There are no conflicts of interest to declare.

Acknowledgements

This work was supported in part by the National Natural Science Foundation of China (NSFC) (No. 82272138, 81971738, 52073258), Outstanding Youth Foundation of Jiangsu Province of China (BK20220086), the Double First Class Fund, China Pharmaceutical University (CPUQNJC22_03), the Natural Science Foundation of Zhejiang Province (No. LR22E010001, LY20E020017), and the Fundamental Research Funds for the Provincial Universities of Zhejiang (No. RF- B2022006).

References

1 R. L. Siegel, K. D. Miller, H. E. Fuchs and A. Jemal, *CA Cancer J. Clin.*, 2021, **71**, 7–33.
2 N. M. Kuderer, A. Desai, M. B. Lustberg and G. H. Lyman, *Nat. Rev. Clin. Oncol.*, 2022, **19**, 681–697.
3 F. Scotté, R. Ratta and P. Beuzeboc, *Curr. Opin. Oncol.*, 2019, **31**, 280–285.
4 D. Kim, K. Shin, S. G. Kwon and T. Hyeon, *Adv. Mater.*, 2018, **30**, 1802309.
5 W. Fan, B. Yung, P. Huang and X. Chen, *Chem. Rev.*, 2017, **117**, 13566–13638.
6 L. Yu, X. Y. Yu and X. Lou, *Adv. Mater.*, 2018, **30**, e1800939.
7 J. Wang, B. Zhang, J. Sun, W. Hu and H. Wang, *Nano Today*, 2021, **38**, 101146.
8 M. Vallet-Regí, F. Schüth, D. Lozano, M. Colilla and M. Manzano, *Chem. Soc. Rev.*, 2022, **51**, 5365–5451.
9 P. P. Pednekar, S. C. Godiyal, K. R. Jadhav and V. J. Kadam, in *Nanostructures for Cancer Therapy*, Elsevier, 2017, pp. 593–621.
10 N. Singh, A. Karambelkar, L. Gu, K. Lin, J. S. Miller, C. S. Chen, M. J. Sailor and S. N. Bhatia, *J. Am. Chem. Soc.*, 2011, **133**, 19582–19585.
11 I. I. Slowing, J. L. Vivero-Escoto, C.-W. Wu and V. S.-Y. Lin, *Adv. Drug Delivery Rev.*, 2008, **60**, 1278–1288.
12 M. Song, N. Liu, L. He, G. Liu, D. Ling, X. Su and X. Sun, *Nano Res.*, 2018, **11**, 2796–2808.
13 G. D. Moon, S.-W. Choi, X. Cai, W. Li, E. C. Cho, U. Jeong, L. V. Wang and Y. Xia, *J. Am. Chem. Soc.*, 2011, **133**, 4762–4765.
14 Y. Wen, X. Chen, X. Zhu, Y. Gong, G. Yuan, X. Qin and J. Liu, *ACS Appl. Mater. Interfaces*, 2019, **11**, 43393–43408.
15 L. Guo, I. Panderi, D. D. Yan, K. Szulak, Y. Li, Y.-T. Chen, H. Ma, D. B. Niesen, N. Seeram and A. Ahmed, *ACS Nano*, 2013, **7**, 8780–8793.
16 A. Curcio, A. V. de Walle, E. Benassai, A. Serrano, N. Luciani, N. Menguy, B. B. Manshian, A. Sargsian, S. Soenen and A. Espinosa, *ACS Nano*, 2021, **15**, 9782–9795.
17 S. J. Varapragasam, C. Balasanthiran, A. Gurung, Q. Qiao, R. M. Rioux and J. D. Hoefelmeyer, *J. Phys. Chem. C*, 2017, **121**, 11089–11099.
18 X. Wang, J. Feng, Y. Bai, Q. Zhang and Y. Yin, *Chem. Rev.*, 2016, **116**, 10983–11060.
19 Y. Xia, K. D. Gilroy, H. C. Peng and X. Xia, *Angew. Chem., Int. Ed.*, 2017, **56**, 60–95.
20 K. Cheng, S. Peng, C. Xu and S. Sun, *J. Am. Chem. Soc.*, 2009, **131**, 10637–10644.

21 H. Liang, J. Guo, Y. Shi, G. Zhao, S. Sun and X. Sun, *Biomaterials*, 2021, **268**, 120530.
22 A. C. Poulose, S. Veeranarayanan, M. S. Mohamed, Y. Nagaoka, R. R. Aburto, T. Mitcham, P. M. Ajayan, R. R. Bouchard, Y. Sakamoto, Y. Yoshida, T. Maekawa and D. S. Kumar, *Nanoscale*, 2015, **7**, 8378–8388.
23 X. Gong, Y. Yang and S. Huang, *J. Phys. Chem. C*, 2010, **114**, 18073–18080.
24 L. S. Lin, T. Huang, J. Song, X. Y. Ou, Z. Wang, H. Deng, R. Tian, Y. Liu, J. F. Wang, Y. Liu, G. Yu, Z. Zhou, S. Wang, G. Niu, H. H. Yang and X. Chen, *J. Am. Chem. Soc.*, 2019, **141**, 9937–9945.
25 L. Zhang, S. S. Wan, C. X. Li, L. Xu, H. Cheng and X. Z. Zhang, *Nano Lett.*, 2018, **18**, 7609–7618.
26 H. Ranji-Burachaloo, P. A. Gurr, D. E. Dunstan and G. G. Qiao, *ACS Nano*, 2018, **12**, 11819–11837.
27 P. Tsvetkov, S. Coy, B. Petrova, M. Dreishpoon, A. Verma, M. Abdusamad, J. Rossen, L. Joesch-Cohen, R. Humeidi, R. D. Spangler, J. K. Eaton, E. Frenkel, M. Kocak, S. M. Corsello, S. Lutsenko, N. Kanarek, S. Santagata and T. R. Golub, *Science*, 2022, **375**, 1254–1261.
28 S. J. Dixon, K. M. Lemberg, M. R. Lamprecht, R. Skouta, E. M. Zaitsev, C. E. Gleason, D. N. Patel, A. J. Bauer, A. M. Cantley, W. S. Yang, B. Morrison 3rd and B. R. Stockwell, *Cell*, 2012, **149**, 1060–1072.
29 A. Aranda, L. Sequedo, L. Tolosa, G. Quintas, E. Burello, J. V. Castell and L. Gombau, *Toxicol. in Vitro*, 2013, **27**, 954–963.
30 D. V. Krysko, A. D. Garg, A. Kaczmarek, O. Krysko, P. Agostinis and P. Vandenabeele, *Nat. Rev. Cancer*, 2012, **12**, 860–875.
31 H. Deng, Z. Zhou, W. Yang, L. S. Lin, S. Wang, G. Niu, J. Song and X. Chen, *Nano Lett.*, 2020, **20**, 1928–1933.
32 M. Kendall and I. Lynch, *Nat. Nanotechnol.*, 2016, **11**, 206–210.